Acta Cryst. (1997). A53, 426-435

A General Maximum-Entropy Method for Model-Free Reconstructions of Magnetization Densities from Polarized Neutron Diffraction Data

P. SCHLEGER,*† A. PUIG-MOLINA,‡ E. RESSOUCHE, O. RUTTY AND J. SCHWEIZER

Département de la Recherche Fondamentale sur la Matière Condensée/SPSMS/MDN, 17 rue des Martyrs, 38054 Grenoble CEDEX 9, France. E-mail: schleger@ill.fr

(*Received 26 July 1996; accepted 3 February 1997*)

Abstract

A general method for the model-free reconstruction of magnetization densities is presented. The technique is based upon the maximum-entropy principle and is valid for systems with any space-group symmetry, any physically reasonable ordered moment and allows for the incorporation of relevant corrections such as extinction. Thus, it is possible, for the first time, to reconstruct the real-space magnetization densities *in essentially any physical system* exhibiting a ferromagnetic spin alignment (either natural or induced) from polarized neutron diffraction experiments. The technique is illustrated for the purely organic ferromagnet, β-4,4,5,5-tetramethyl-2-*p*-(nitrophenyl)-3-oxido-4,5-dihydroimidazolium 1-oxyl.

1. Introduction

Entropy maximization and Bayesian inference have become powerful tools for solving reconstruction problems given incomplete and/or noisy information. They are of fundamental importance, forming the basis for statistical mechanics (*e.g.* Grandy, 1989; Gzyl, 1995) and play an important role in the analysis of experimental data from a wide variety of fields, such as astronomy, medicine, economics and condensed-matter physics (*e.g.* Smith & Grandy, 1985; Erickson & Smith, 1988; Skilling, 1989; Mohammad-Djafari & Demoments, 1993).

In neutron and X-ray scattering, one is essentially faced with the problem of the (complex) Fourier inversion of a limited set of noisy data in order to find the corresponding real-space scattering density. Moreover, there is usually an additional loss of information through the intervening non-linearity relating the measurement to the Fourier coefficients. For example, the Fourier transform of the real-space charge distribution gives the corresponding X-ray structure factor, but X-ray diffraction only measures its magnitude not its phase. There is obviously no unique solution to such problems.

Of course, one possibility is to develop a model describing the real-space scattering density whose parameters are optimized to fit the experiment. This is often difficult, however. Furthermore, features that a model does not account for, but are contained in the data, will not be revealed. Thus, it is desirable to have a model-free§ tool that gives a relatively unbiased real-space representation of the reciprocal-space measurements.

Since the model-free solution is not unique, in a sense, the best one can do is to try and find the most *reasonable* map whose Fourier transform is *consistent* with the experimental data. Crudely speaking, the maximum-entropy (MAXENT) principle provides a definition of what is 'reasonable' and the scheme for selecting the 'best' map.¶ A variety of techniques can be used for finding the MAXENT solution. Many are restricted to linear reconstruction problems, where the Fourier coefficients are directly measurable (*e.g.* Zhuang, Östevold & Haralick, 1987; Sakata & Sato, 1990; Kumazawa, Kubota, Takata & Sakata, 1993; Sakata, Uno, Takata & Howard, 1993; De Vries, Briels & Feil, 1994; Steenstrup & Hansen, 1994; Takata, Sakata, Kumazawa, Larsen & Iversen, 1994; Kumazawa, Takata & Sakata, 1995) or are specialized to the phase problem in crystallography (*e.g.* Wilkins, Varghese & Lehmann, 1983; Wilkins, 1983; Navaza, 1985; Bricogne & Gilmore, 1990; Gilmore, Bricogne & Bannister, 1990). Skilling & Bryan (1984) have developed a powerful algorithm capable of dealing with quite general *non-linear* reconstructions, where the (Fourier) transform of the map is not linearly related to the experimental data. This 'Cambridge' MAXENT algorithm, as well as a more recent variant by Bryan (1990), however, are restricted to *real* transforms.

The reconstruction of spin densities for centrosymmetric crystals is essentially a straightforward Fourier-inversion problem and MAXENT has been successfully applied to this (*e.g.* Papoular & Gillon, 1990; Papoular, Ressouche, Schweizer & Zheludev, 1993; Zheludev, Papoular, Ressouche & Schweizer, 1995). For non-centrosymmetric crystal structures, the situation is more complicated:

† Present address: Institut Laue–Langevin, BP 156, 38042 Grenoble CEDEX 9, France.

‡ Present address: European Synchrotron Radiation Facility, BP 220, 38042 Grenoble CEDEX 9, France.

§ Model free in the sense that it is independent of atomicity and chemical bonding assumptions.

¶ A more careful interpretation is given by Bryan (1990).

The neutron intensity of a Bragg reflection is determined by the nuclear $\tilde{n}_k = n'_k + in''_k$ and magnetic $\tilde{m}_k = m'_k + im''_k$ structure factors (we will denote complex variables by a tilde). The index k refers to a particular Bragg reflection defined by the Miller indices and runs from 1 to M_0, corresponding to the number of measured reflections. The crystal structure is known so that the nuclear structure factors are given. In a polarized neutron diffraction experiment, one measures the ratio of the Bragg intensity for incident 'spin-up' and 'spin-down' polarized neutron beams (Gillon & Schweizer, 1989). If the sample has a ferromagnetic spin alignment (natural or induced), collinear with the incident neutron spin polarization,* then the flipping ratio f_k is given by (Gillon & Schweizer, 1989; Zheludev, Bonnet *et al.*, 1994)

$$f_k = \frac{|\tilde{n}_k|^2 + q_k^2|\tilde{m}_k|^2 + 2q_k^2 p(m'_k n'_k + m''_k n''_k)}{|\tilde{n}_k|^2 + q_k^2|\tilde{m}_k|^2 - 2q_k^2 \varepsilon p(m'_k n'_k + m''_k n''_k)}, \quad (1)$$

where q_k is related to the angle between the alignment of the unpaired spin in the sample and the scattering vector $\mathbf{Q}$, p is the neutron polarization ($p \leq 1$) and ε is the flipping efficiency. Since the Fourier transform of the spin density is the magnetic structure factor, the flipping ratio contains information about the spin density. However, in non-centrosymmetric crystals, the imaginary part of $\tilde{m}_k$ is non-zero and it is not possible to extract from the flipping ratio the two unknowns necessary for the Fourier inversion of $\tilde{m}_k$. Thus, the spin-density reconstruction in non-centrosymmetric crystals does not reduce to a linear Fourier inversion.

The strategy of Papoular & Delapalme (1994) attempts to circumvent this difficulty by approximating (1) with a first-order Taylor-series expansion in $\tilde{\mathbf{m}}$. This reduces the problem to a linear Fourier inversion and they are able simply to apply the existing Cambridge algorithm. The catch, however, is that, for a flipping ratio of $f = 1 + \Delta f$, the second-order term in the expansion of (1) is roughly $(\Delta f)^2/2$. For a measured flipping ratio of 1.4, the error is thus already 20%. In order to limit the artifacts introduced by the approximation, one is required to exclude any measured flipping ratios outside the interval $0.6 \leq f^0 \leq 1.4$ (which is probably quite optimistic). But, the more a flipping ratio deviates from unity, the more it is dominated by magnetic scattering. The end effect is that one is forced to discard those data with the greatest amount of magnetic information! Since neutron scattering is an intensity-limited experimental technique, one cannot afford to throw away the best data. Finally, this approach does not easily allow for the inclusion of the usual corrections such as extinction, $\lambda/2$ contamination, nuclear polarization *etc.*; for each correction, one must examine the validity of the linearization scheme.

* Note that in order to define the spin orientation and/or to create a ferromagnetic spin component, a magnetic field is applied perpendicular to the scattering plane.

The motivation to develop an algorithm able to use the correct functional form [*i.e.* (1)] is thus quite clear. In the next section, we outline how the existing algorithms may be generalized to handle the case of a complex (Fourier) transform, with an intervening non-linearity between the Fourier coefficients and the experimental data. §3 then applies this to the spin-density reconstruction of β-4,4,5,5-tetramethyl-2-(*p*-nitrophenyl)-3-oxido-4,5-dihydroimidazolium 1-oxyl and compares the model-free MAXENT reconstruction to the results of a multipole-expansion fit. We also illustrate how to use MAXENT to test the validity of a proposed model. Finally, §4 concludes the paper with a brief discussion of some remaining difficulties.

2. The MAXENT formalism

Maximum-entropy algorithms are abundantly available in the literature, so we will not repeat the full details here but simply point out the essential elements that are distinct from those for the linear reconstruction problem. To that effect, we outline the linear case with real transforms and then gradually introduce more general situations indicating the steps necessary for dealing with the more complicated case.

In practice, one discretizes a map into N_0 pixels, so that a particular map can be viewed as a vector $\boldsymbol{\rho}$, where the jth vector component corresponds to the average real-space density within the jth pixel. The MAXENT reconstruction is obtained by finding the global unconstrained maximum of

$$Q(\boldsymbol{\rho}) = \alpha S(\boldsymbol{\rho}) - \tfrac{1}{2} C(\boldsymbol{\rho}), \quad (2)$$

where S is the appropriate entropy functional, C is the regular χ^2 goodness-of-fit measure (see §2.1) and α is a positive Lagrange multiplier. In 'historic' maximum entropy (Gull & Daniel, 1978; Gull & Skilling, 1984), α is used *ad hoc* as an approach or regularizing parameter but it may also be calculated self-consistently (Gull, 1988).

In the case where $\rho_j > 0$, the entropy is given by (Skilling, 1988)

$$S(\boldsymbol{\rho}) = \sum_{j=1}^{N_0} \rho_j - \mu_j - \rho_j \ln(\rho_j/\mu_j), \quad (3)$$

where μ_j is a prior map relative to which the entropy is defined. In the absence of the experimental data, the map reconstruction $\boldsymbol{\rho}$ remains the prior map $\boldsymbol{\mu}$. Any information known *before* the experiment can be incorporated into the prior map, but often $\boldsymbol{\mu}$ is chosen to be a constant.

The χ^2 constraint is closely linked to the type of experiment and the particular transformation connecting the (real-space) map to the (reciprocal-space) data. Thus,

our focus will be on the form of $C(\rho)$ for different types of experiments.

First, we define the transformation between image space and data space by an $M_0 \times N_0$ matrix $\mathbf{R}$ so that the data-space representation $\mathbf{m}$ of the image ρ is

$$m_k = \sum_{j=1}^{N_0} R_{kj}\rho_j \tag{4}$$

or, equivalently,

$$\mathbf{m} = \mathbf{R}\rho. \tag{5}$$

In the case where the transform $\mathbf{R}$ is complex, since the image-space density map is still real, one can define $\mathbf{R}$ as a $2M_0 \times N_0$ matrix, where the first M_0 rows correspond to the real part of the transform and the second half to the imaginary part. Similarly, a *complex* data-space vector $\tilde{\mathbf{m}}$ becomes a vector with $2M_0$ entries, with the real part retained in the first M_0 entries and the imaginary part in the rest. With this notation and storage convention, (5) becomes identical for real and complex transforms.

2.1. *Real linear mapping*

If the kth observation is denoted m_k^0 with an associated uncertainty σ_k, the χ^2 constraint is

$$C(\rho) = \sum_{k=1}^{M_0} w_k^2 \left(m_k^0 - \sum_{j=1}^{N_0} R_{kj}\rho_j \right)^2. \tag{6}$$

Here, w_k is the weighting factor equal to $1/\sigma_k$. If the weighted residuals are defined as a vector with M_0 elements (square brackets denote a diagonal matrix)

$$\mathbf{r} = [\mathbf{w}](\mathbf{m^0} - \mathbf{R}\rho), \tag{7}$$

the constraint function is simply

$$C(\rho) = \mathbf{r}^T\mathbf{r}. \tag{8}$$

All iterative algorithms are essentially based upon an expansion of $Q(\rho)$ for arbitrary small variations $\delta\rho$. Focusing on $C(\rho + \delta\rho)$ and expanding to second order in $\delta\rho$, one obtains

$$\begin{aligned} C(\rho + \delta\rho) \simeq C(\rho) &- 2\delta\rho^T\mathbf{R}^T[\mathbf{w}]\mathbf{r} \\ &+ \delta\rho^T\mathbf{R}^T[\mathbf{w}][\mathbf{w}]\mathbf{R}\delta\rho. \end{aligned} \tag{9}$$

Correspondingly, an expansion of the entropy gives

$$S(\rho + \delta\rho) \simeq S(\rho) + \delta\rho^T \log(\rho/\mu) - \tfrac{1}{2}\delta\rho^T[\rho^{-1}]\delta\rho. \tag{10}$$

The simplest algorithm relies only on the first-order term and is sometimes called the 'single-pixel approximation' (*e.g.* Gull & Daniel, 1978; Wilkins, 1983; Sakata & Sato, 1990; Sakata, Uno, Takata & Howard, 1993; Kumazawa, Takata & Sakata, 1995). These can be quite slowly converging and unstable, so that second-order variants exist (*e.g.* Wilkins, Varghese & Lehmann, 1983; Skilling & Bryan, 1984; Gull & Skilling, 1989; Bryan, 1990; De Vries, Briels & Feil, 1994).

The condition for a maximum (*i.e.* $\alpha\nabla S - \frac{1}{2}\nabla C = 0$) gives

$$\rho = \mu \exp(\mathbf{R}^T\alpha^{-1}[\mathbf{w}]\mathbf{r}). \tag{11}$$

Typically, one chooses to reconstruct a map with high resolution so that the number of pixels usually greatly exceeds the number of data points. Since (11) must hold, it is more efficient to iterate in 'data space' by introducing a new variable $\mathbf{u}$, which is related to the map by

$$\rho = \mu \exp(\mathbf{R}^T\mathbf{u}). \tag{12}$$

From the quadratic model for S and C, one can derive an iterative equation for $\mathbf{u}$ (Gull & Skilling, 1989; Bryan, 1990) ($\mathbf{I}$ is the identity matrix):

$$\delta\mathbf{u} = [\mathbf{w}](\beta\mathbf{I} + \mathbf{A})^{-1}\mathbf{g}, \tag{13}$$

with

$$\mathbf{A} = [\mathbf{w}]\mathbf{R}[\rho]\mathbf{R}^T[\mathbf{w}], \quad \mathbf{g} = -\alpha[\mathbf{w}^{-1}]\mathbf{u} + \mathbf{r}. \tag{14}$$

The second-order expansion in $\delta\rho$ is only valid for small step sizes, so the constant β ($\geq\alpha$) has been introduced to restrict the increments (Skilling & Bryan, 1984; Gull & Skilling, 1989; Bryan, 1990). As initial condition, one chooses $\mathbf{u} = 0$ and α very large. $\mathbf{u} = 0$ corresponds to the MAXENT solution in the absence of experimental data ($\rho = \mu$) and a large α validates this choice by making C irrelevant [equation (2)]. The iteration then proceeds by succesive applications of δu and simultaneous reductions of α and β. After each iteration, the actual map ρ is calculated from (12). For more details, we refer the reader to Skilling & Bryan (1984), Gull & Skilling (1989) and Bryan (1990), and note in passing that that the bulk of the computational work is in finding the inverse of the $M_0 \times M_0$ *symmetric* matrix $(\beta\mathbf{I} + \mathbf{A})$. Next, we examine how (13) may take a different form under more general conditions.

2.2. *Complex linear mapping*

In the case where $\mathbf{R}$ is no longer real but complex, *i.e.* $\tilde{\mathbf{R}}_{kj} = \mathbf{R}'_{kj} + i\mathbf{R}''_{kj}$, the image-data transform of (5) will produce, in principle, a complex number, so that $\tilde{m}_k = m'_k + im''_k$:

$$\begin{aligned} m'_k &= \sum_j R'_{kj}\rho_j \\ m''_k &= \sum_j R''_{kj}\rho_j. \end{aligned} \tag{15}$$

With the assumption that one can measure the real and imaginary parts of $\tilde{m}_k^0$, the appropriate constraint function is now

$$C = \sum_k w_k^2 |\tilde{m}_k - \tilde{m}_k^0|^2, \tag{16}$$

which, if written out explicitly, becomes

$$C = \sum_k w_k^2 [(m_k' - m_k^{0\prime})^2 + (m_k'' - m_k^{0\prime\prime})^2]. \tag{17}$$

If we store a complex vector as a real vector, with double the number of elements, identifying the first half with the real part and the second half with the imaginary part, then (17) becomes essentially identical to (8), hence (13) is unchanged except that data-space variables have twice as many elements. Thus, one can apply the same algorithms as for real transforms.

2.3. *Real non-linear mapping*

What happens when one has a real transform but the measured variable is no longer a linear functional of the density map? Suppose that we have a linear real transform between the density map and some data-space quantity, as in (5), but the quantity measured is no longer directly m_k but a function $f_k = f(m_k)$ with measurements f_k^0. Furthermore, let us assume that $f(m_k)$ is real. Then the constraint function is

$$C = \sum_k w_k^2 [f_k^0 - f(m_k)]^2 \tag{18}$$

or, in vectorized form,

$$C(\mathbf{f}) = \Big(\mathbf{f}^0 - f(\mathbf{R}\rho)\Big)^T [\mathbf{w}^2] \Big(\mathbf{f}^0 - f(\mathbf{R}\rho)\Big). \tag{19}$$

A Taylor-series expansion of $C(\rho + \delta\rho)$ to second order in $\delta\rho$ gives

$$\begin{aligned} C(\rho + \delta\rho) \simeq C(\rho) &- 2\delta\rho^T \mathbf{R}^T [\partial\mathbf{f}][\mathbf{w}]\mathbf{r} \\ &+ \delta\rho^T \mathbf{R}^T [\partial\mathbf{f}][\mathbf{w}^2][\partial\mathbf{f}]\mathbf{R}\delta\rho \\ &- \delta\rho^T \mathbf{R}^T [\partial^2\mathbf{f}][\mathbf{w}][\mathbf{r}]\mathbf{R}\delta\rho, \end{aligned} \tag{20}$$

where $\partial\mathbf{f} = \partial f(\mathbf{m})/\partial\mathbf{m}$ and $\partial^2\mathbf{f} = \partial^2 f(\mathbf{m})/\partial\mathbf{m}^2$. If the last term in (20) is neglected, then a simple rescaling of the weights $\mathbf{w}$ by $\partial\mathbf{f}$ re-casts the expansion into an identical form as for the linear case, so that the same iterative algorithms may be retained. Explicitly, one writes $[\partial\mathbf{f}][\mathbf{w}] = [\hat{\mathbf{w}}]$ and (20) becomes

$$\begin{aligned} C(\rho + \delta\rho) \simeq C(\rho) &- 2\delta\rho^T \mathbf{R}^T [\hat{\mathbf{w}}]\mathbf{r} \\ &+ \delta\rho^T \mathbf{R}^T [\hat{\mathbf{w}}][\hat{\mathbf{w}}]\mathbf{R}\delta\rho \end{aligned} \tag{21}$$

and (13) is unchanged.

On the one hand, the neglect of the last term in the expansion obviously does not alter the definition of an extremum, so that as long as the iteration progresses a MAXENT solution will be found. Furthermore, as the fit progresses, the residuals $\mathbf{r}$ decrease and this last term should rapidly loose importance. On the other hand, much more severely, the introduction of the non-linearity $f(\mathbf{R}\rho)$ can render the MAXENT solution non-unique (Wilkins, Varghese & Lehmann, 1983). In order to apply the above to such a situation, it would be necessary to have some prior knowledge that could be incorporated into the reference map. Otherwise, more sophisticated techniques should be applied (*e.g.* Bricogne & Gilmore, 1990; Gilmore, Bricogne & Bannister, 1990).

2.4. *Complex non-linear mapping*

Now we consider practically the most general case, where the transform is complex and the measured variable is a non-linear functional of the map. The appropriate constraint function becomes

$$C(\rho) = \Big(\mathbf{f}^0 - f(\mathbf{m}', \mathbf{m}'')\Big)^T [\mathbf{w}^2] \Big(\mathbf{f}^0 - f(\mathbf{m}', \mathbf{m}'')\Big), \tag{22}$$

where now f is a function of *two* variables, the real and imaginary parts of the complex transform, $\mathbf{m}'$ and $\mathbf{m}''$, defined by (15). Thus, one needs to make a two-dimensional Taylor-series expansion of $f(\mathbf{m}', \mathbf{m}'')$. Under the same assumption as that leading to (21), *i.e.* that one can neglect any second-order terms proportional to the residuals, we only need to expand $f(\mathbf{m}', \mathbf{m}'')$ to first order. After some algebra to cast the expansion into the most compact form, one obtains

$$\begin{aligned} C(\rho + \delta\rho) \simeq C(\rho) &- 2\delta\rho^T \tilde{\mathbf{R}}^T [\tilde{\mathbf{w}}]\tilde{\mathbf{r}} \\ &+ 2\delta\rho^T \tilde{\mathbf{R}}^T [\tilde{\mathbf{w}}]\mathbf{S}[\tilde{\mathbf{w}}]\tilde{\mathbf{R}}\delta\rho, \end{aligned} \tag{23}$$

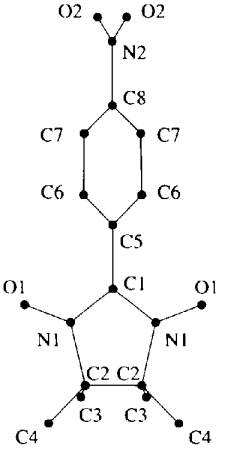

Fig. 1. Atom numbering scheme for 3-4,4,5,5-tetramethyl-2-(*p*-nitrophenyl)-3-oxido-4,5-dihydroimidazolium 1-oxyl.

where the weights are redefined as

$$\tilde{\mathbf{w}} = \begin{pmatrix} [\mathbf{w}]\partial\mathbf{f}/\partial\mathbf{m}' \\ [\mathbf{w}]\partial\mathbf{f}/\partial\mathbf{m}'' \end{pmatrix} \equiv \begin{pmatrix} [\mathbf{w}]\partial\mathbf{f}' \\ [\mathbf{w}]\partial\mathbf{f}'' \end{pmatrix} \tag{24}$$

and the 'complex' residuals have equal real and imaginary parts:

$$\tilde{\mathbf{r}} = \begin{pmatrix} \mathbf{r} \\ \mathbf{r} \end{pmatrix}. \tag{25}$$

The complex transform $\tilde{\mathbf{R}}$ is, as described in §2, a $2M_0 \times N_0$ matrix:

$$\tilde{\mathbf{R}} = \begin{pmatrix} \mathbf{R}' \\ \mathbf{R}'' \end{pmatrix}. \tag{26}$$

The only difference now is that there is an additional operator $2\mathbf{S}$ in the second-order term of the expansion. $\mathbf{S}$ arises owing to the existence of cross terms that multiply real and imaginary parts of the complex transforms. The matrix $\mathbf{S}$, operating on a complex vector $\tilde{\mathbf{v}}$, averages the real and imaginary parts and is defined as

$$\mathbf{S}\tilde{\mathbf{v}} = \mathbf{S}\begin{pmatrix} \mathbf{v}' \\ \mathbf{v}'' \end{pmatrix} = \begin{pmatrix} (\mathbf{v}' + \mathbf{v}'')/2 \\ (\mathbf{v}' + \mathbf{v}'')/2 \end{pmatrix}. \tag{27}$$

Note that $\mathbf{SS}\tilde{\mathbf{v}} = \mathbf{S}\tilde{\mathbf{v}}$ and $\mathbf{S}^T = \mathbf{S}$.

Thus, it is in principle possible to retain the same algorithms, with only two modifications: data-space vectors become complex quantities, doubling their storage requirements, and the evaluation of the last term in the expansion must include the matrix $\mathbf{S}$. In particular, the matrix $\mathbf{A}$ and vector $\mathbf{g}$ [equation (14)] of the data-space algorithm become

$$\begin{aligned} \mathbf{A} &= 2\mathbf{S}[\tilde{\mathbf{w}}]\tilde{\mathbf{R}}[\rho]\tilde{\mathbf{R}}^T[\tilde{\mathbf{w}}]\mathbf{S} \\ \tilde{\mathbf{g}} &= -\alpha[\tilde{\mathbf{w}}^{-1}]\mathbf{u} + \tilde{\mathbf{r}}. \end{aligned} \tag{28}$$

An important point to note is that $\mathbf{A}$ remains a symmetric matrix. Thus, only a simple modification to the evaluation of $\mathbf{A}$ in the computer code is necessary to generalize the algorithm for the complex non-linear case. Whether the iteration actually converges and whether a unique solution exists depends on the specific form of the non-linearity in f. For example, this approach does not work for phaseless (neutron or X-ray) structure-factor data with a uniform prior map, μ = constant. The spin-density reconstruction problem, however, where the magnetic contribution to the scattering is typically smaller than the nuclear part, seems not to suffer from convergence problems.

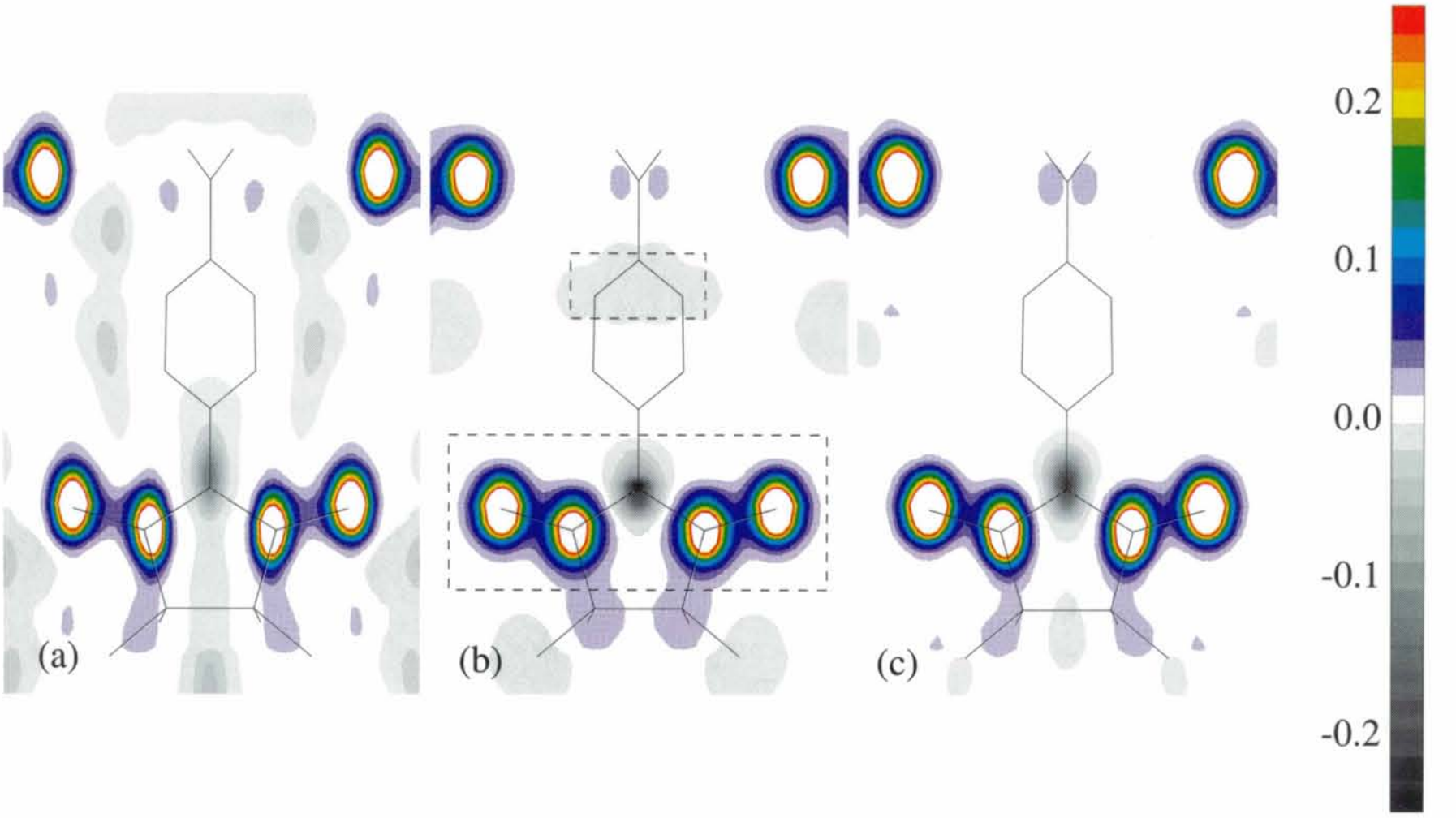

Fig. 2. Main view of the magnetization density as reconstructed by (*a*) MAXENT with uniform prior, (*b*) multipole expansion of Zheludev, Bonnet *et al.* (1994), and (*c*) MAXENT with multipole expansion as non-uniform prior. The solid lines indicate the principal bonding within the molecule. The lower and upper dotted boxes indicate the regions displayed in Figs. 3 and 4, respectively. Note that the scale is in units of μ_B Å^{-2}.

3. Application to flipping ratios from polarized neutron experiments

The task of extracting spin densities from the flipping ratios measured by polarized neutron diffraction of a *known* non-centrosymmetric structure is exactly the case described in §2.4. In the absence of systematic corrections, the flipping-ratio measurements are related to the magnetic structure factor *via* (1). For the algorithm, we require the derivatives of f_k, which rescale the weights $\tilde{\mathbf{w}}$:

$$\frac{\partial f_k}{\partial m'} = \frac{2q_k^2 p(1+\varepsilon)(n'_k a_k - m'_k b_k)}{(a_k - \varepsilon p b_k)^2} \tag{29}$$

$$\frac{\partial f_k}{\partial m''} = \frac{2q_k^2 p(1+\varepsilon)(n''_k a_k - m''_k b_k)}{(a_k - \varepsilon p b_k)^2}, \tag{30}$$

where

$$a_k = |n_k|^2 + q_k^2 |m_k|^2 \tag{31}$$

$$b_k = 2q_k^2 (m'_k n'_k + m''_k n''_k). \tag{32}$$

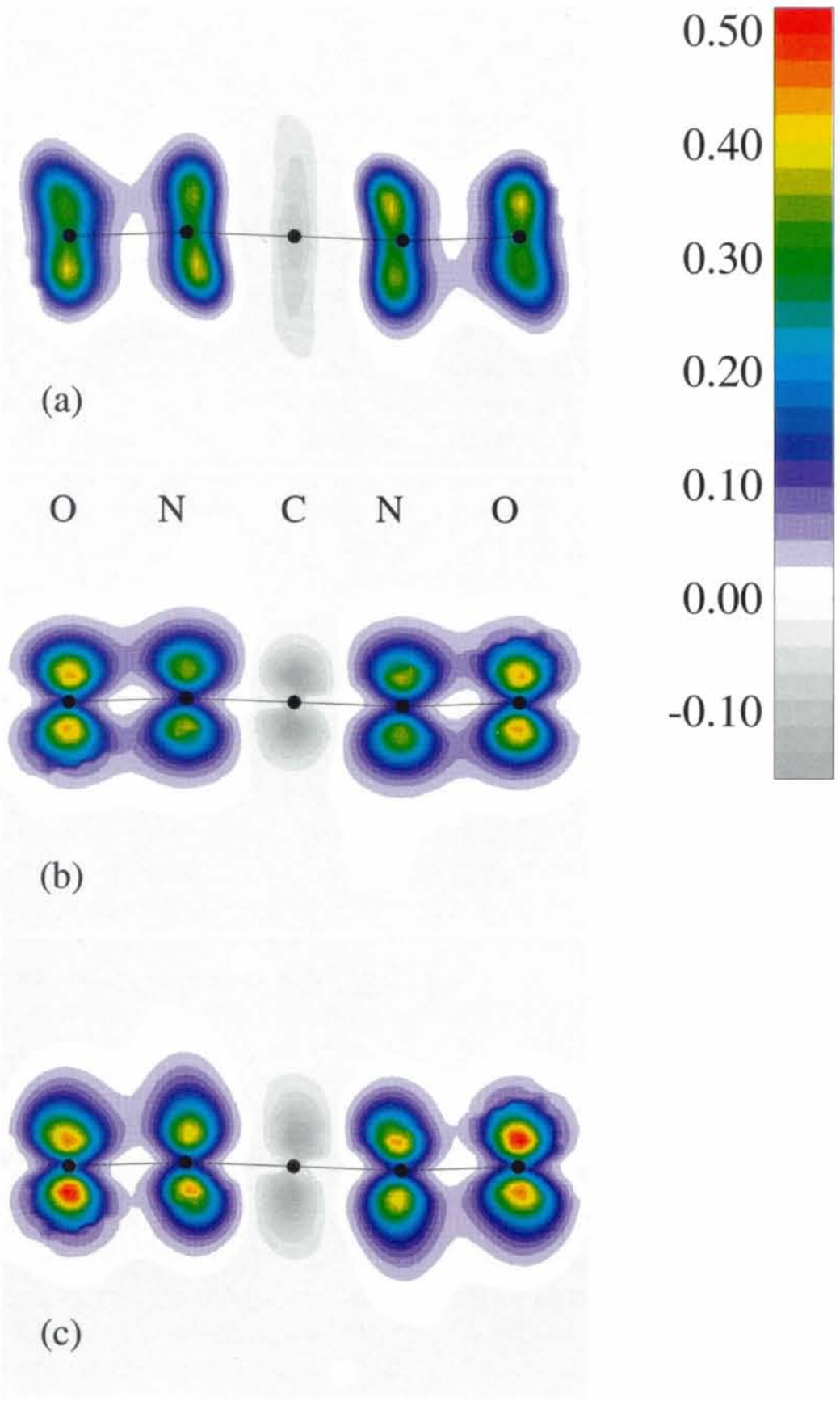

Fig. 3. View onto the O—N—C—N—O fragment, rotated with respect to Fig. 2 by 90° about the horizontal. (*a*), (*b*) and (*c*) refer to the same reconstructions as in Fig. 2.

One may also take into account systematic corrections such as $\lambda/2$ contamination or extinction. In the case of secondary type-II extinction, the flipping ratio becomes

$$f_k = f_k^{\text{uncor}}[y(a_k + pb_k)/y(a_k - \varepsilon pb_k)] \qquad (33)$$

with f_k^{uncor} given by (1) and $y(x)$ is the extinction correction given by Becker & Coppens (1974):

$$y(x) = \{1 + C_1 x + [C_2 x^2/(1 + C_3 x)]\}^{-1/2}. \qquad (34)$$

The variables C_1, C_2 and C_3 depend upon the scattering angle, the effective neutron path length through the sample, the neutron wavelength, the lattice constants and an extinction parameter g.

It should be noted that spin densities may be positive or negative (*i.e.* ρ_j is not positive definite) so that the entropy functional (3) must be modified. Various suggestions have been made (Sakata, Uno, Takata & Howard, 1993; Gull & Skilling, 1989; Steenstrup & Hansen, 1994) and our spin-density reconstructions are based on the *MEMSYS*III subroutine library (Gull & Skilling, 1989), which we have modified to handle the complex non-linear case. It treats the case of non-positive-definite distributions by assuming that a map may be expressed as the difference between two subsidiary positive-definite distributions, leading to a modified form for S (Gull & Skilling, 1989). Since this modifies the details of the iterative equations, but not the general approach, we do not repeat the details here but refer the reader to Gull & Skilling (1989).

3.1. *Spin-density reconstruction of β-4,4,5,5-tetramethyl-2-(p-nitrophenyl)-3-oxido-4,5-dihydroimidazolium 1-oxyl*

We illustrate the power of this technique on the purely organic ferromagnet β-4,4,5,5-tetramethyl-2-(*p*-nitrophenyl)-3-oxido-4,5-dihydroimidazolium 1-oxyl (see Fig. 1 for a schema of the molecule), whose flipping ratios were first measured by Zheludev, Bonnet *et al.* (1994), and analyzed using a parametrized multipole expansion as a model. An important feature of this data set is that the crystal exhibited significant secondary type-II extinction. Note that the effect of extinction on the flipping ratios is always to bring the measured values closer to one. Thus, a neglect of extinction in the analysis will tend to result in weaker spin densities.

4,4,5,5-Tetramethyl-2-(*p*-nitrophenyl)-3-oxido-4,5-di-hydroimidazolium 1-oxyl (*p*-NPNN) is the first purely organic ferromagnet (Kinoshita, 1993). It belongs to the family of nitronyl nitroxide free radicals in which one unpaired electron is expected to be delocalized mainly over the two NO groups of the nitronyl fragment.

The β phase of *p*-NPNN crystallizes in *Fdd*2, a non-centrosymmetric orthorhombic space group. Its Curie temperature was determined to be $T_c = 0.67$ K by specific heat (Nakazawa *et al.*, 1992) and zero-field muon spin rotation (Le *et al.*, 1993). The ferromagnetic nature of the magnetic structure was clearly confirmed by zero-field unpolarized neutron diffraction (Zheludev, Ressouche, Schweizer & Turek, 1994).

The flipping ratios in β-*p*-NPNN were measured on a single crystal by Zheludev, Bonnet *et al.* (1994), in an applied field $H = 4.65$ T at low temperature ($T = 1.6$ and 2.0 K) but still in the paramagnetic phase. With this method, it was not necessary to reach the ferromagnetic phase, since the applied field was sufficiently strong to induce a ferromagnetic component of the spin density in the paramagnetic phase. The 'flipping ratios' $f(h, k, l)$ were measured for 246 Bragg reflections, using a lifting counter spectrometer.

We performed the reconstruction on a $32 \times 32 \times 32$ grid in the asymmetric unit of the *Fdd*2 space group. Fig. 2 compares the MAXENT reconstruction with a uniform prior (Fig. 2*a*) with the multipole expansion of Zheludev, Bonnet *et al.* (1994) (Fig. 2*b*). It is important to realize that, whereas the model *imposes* a certain physical solution, *the MAXENT reconstruction is obtained with only the experimental information and the space group.* The qualitative features are the same, with the main spin density centered on the N—O free radicals; even the *p*-orbital symmetry is clearly reproduced (Fig. 3). In detail, however, some differences are clear: In the projection onto the O—N—C—N—O molecular plane, the model forces a spherically symmetric spin density, whereas MAXENT finds it to be more anisotropic. Furthermore, the lobes do not have equal weight. Finally, we note that a significant disagreement exists for the spin density on the C atoms of the nitrophenyl group. Zheludev, Bonnet *et al.* (1994) refined a negative spin density, whereas the MAXENT reconstruction finds this region to be positive (see Fig. 4). Although the spin density in this region is very small, we consistently find this result either with or without extinction corrections.

The quality of map reconstructions can be significantly enhanced through the use of a non-uniform prior μ (Zheludev, Papoular, Ressouche & Schweizer, 1995). But, also, MAXENT can be used to check whether a proposed model contains all the features that an experiment may reveal. Thus, a further reconstruction was made using the multipole expansion as a prior map μ. Figs. 2(*c*), 3(*c*) and 4(*c*) show that reconstruction now resembles the fitted model more closely but that the main discrepancies remain. In particular, the spin density on the C7 atom of the nitrophenyl group remains positive (Fig. 4*c*). This suggests that either the data contains additional systematic errors that must be included in (33) or that these differences should be considered significant. An argument supporting this is the fact that apparent artifacts of equivalent spin density visible in Fig. 2(*a*) vanish when the non-uniform prior map is used, whereas the positive spin density in Fig. 4(*a*) remains. Although

there are other corrections that could be included, such as $\lambda/2$ contamination, it seems unlikely, for example, that their neglect would give rise to systematic features such as the positive spin density on the C7 atoms. This calls into question the intermolecular exchange interaction proposed (Zheludev, Bonnet *et al.*, 1994), since it relies on a negative spin density here.

Looking at the difference between the non-uniform prior map and the reconstruction reveals other weaknesses in the model: Fig. 5 clearly shows that unpaired p-orbital spins on the N—O free radical are pushed off-center owing to their antibonding character. This nicely illustrates how the MAXENT reconstruction can be used to pinpoint possible deficiencies in a proposed model.

4. Concluding remarks

The main point to emphasize is that it is now possible to obtain real-space magnetization densities from flipping-ratio experiments for virtually any system, without the application of a model. The approach presented here is very general, allowing one to easily incorporate systematic corrections and eliminates the restriction to weak spin systems.

There are some open issues, however, that have yet to be addressed. First, we have not determined whether there exists a unique global maximum of (2) for the spin-density problem or if there are local extrema into which the iterative solution might become locked. A sufficient condition for uniqueness (Wilkins, Varghese & Lehmann, 1983) is that $\rho^T(\nabla\nabla C)\rho \geq 0$ for all possible ρ, *i.e.* that the χ^2 constraint C is convex. For the spin-density problem, this condition can be written in the form

$$\sum_{k=1}^{M_0} u_k^2 + v_k r_k, \tag{35}$$

where u_k and v_k are determined from C. It is clear that, unless the residuals are zero, C is not purely convex, since the second term in (35) may be negative. However, one knows that, for the linear cases described in §§2.1 and 2.2, C is convex (Wilkins, Varghese & Lehmann, 1983). Furthermore, in the *limit* of weak spins, the linearization approximation is accurate. This means that one will have a gradual cross over from a well determined unique solution to the possibility of multiple maxima in Q as the spin density increases: effectively, for sufficiently strong spin densities, the problem becomes similar to the crystallographic phase problem. Preliminary simulations with artificial flipping-ratio data for progressively stronger spin systems show, however, that this does not seem to be a problem. We find that until the magnetic structure factors become *on average* comparable to the nuclear structure factors, qualitatively correct maps are reconstructed. Such an overall domination of the magnetic contribution is not realized in nature, since it requires several tens to hundreds of bohr magnetons per atom.

The extraneous structure found in the MAXENT reconstruction above, in particular in the regions far from the atoms (see Fig. 2*a*), suggests that some minor artifacts do crop up. In light of this, as well as the general criticisms put forward by Jauch & Palmer (1993) and Jauch (1994) concerning MAXENT reconstructions, it is important to view this as a *qualitative* tool, designed to reveal the general spin-density features and as an aid to model development. It is for the latter that we imagine MAXENT to be most useful, helping to suggest an appropriate description and checking existing models for consistency.

In conclusion, we have outlined a generalization of an existing maximum-entropy reconstruction algorithm that encompasses complex transforms as well as non-linear maps. The technique was applied to spin-density reconstructions from polarized neutron scattering experiments, showing that a previously proposed linearization approximation is not necessary for this problem. Furthermore, the formalism allows one to incorporate systematic corrections such as extinction quite easily. This technique provides researchers into neutron scattering for the first time the ability to obtain quickly a qualitative picture of the real-space spin densities, without the application of a model, in any physical system with no restrictions on the space group or the spin-density magnitude. Using a non-uniform prior map, we illustrated how the algorithm may serve as a powerful model development tool, pointing out specific deficiencies and determining when the information contained in an experiment becomes fully consistent with a proposed model.

References

Becker, P. & Coppens, P. (1974). *Acta Cryst.* A**30**, 129–153.

Bricogne, G. & Gilmore, C. J. (1990). *Acta Cryst.* A**46**, 284–297.

Bryan, R. K. (1990). *Eur. Biophys. J.* **18**, 165–174.

De Vries, R. Y., Briels, W. J. & Feil, D. (1994). *Acta Cryst.* A**50**, 383–391.

Erickson, G. J. & Smith, C. R. (1988). Editors. *Maximum Entropy and Bayesian Methods in Science and Engineering*, Vol. 1+2. Dordrecht: Kluwer Academic Publishers.

Gillon, B. & Schweizer, J. (1989). In *Molecules in Physics, Chemistry and Biology*, Vol. III, edited by J. Maruani, pp. 111–147. Dordrecht: Kluwer Academic Publishers.

Gilmore, C. J., Bricogne, G. & Bannister, C. (1990). *Acta Cryst.* A**46**, 297–308.

Grandy, W. T. Jr (1989). *Maximum Entropy and Bayesian Methods*, edited by J. Skilling, pp. 73–92. Dordrecht: Kluwer Academic Publishers.

Gull, S. F. (1988). *Maximum Entropy and Bayesian Methods*, edited by J. Skilling, pp. 53–72. Dordrecht: Kluwer Academic Publishers.

Gull, S. F. & Daniel, G. J. (1978). *Nature (London)*, **272**, 686–690.
Gull, S. F. & Skilling, J. (1984). *IEE Proc.* **131**(F), 646–650.
Gull, S. F. & Skilling, J. (1989). *MEMSYSIII Quantified Maximum Entropy Subroutine Library*. Meldreth, United Kingdom.
Gzyl, H. (1995). *The Method of Maximum Entropy*. Singapore: World Scientific.

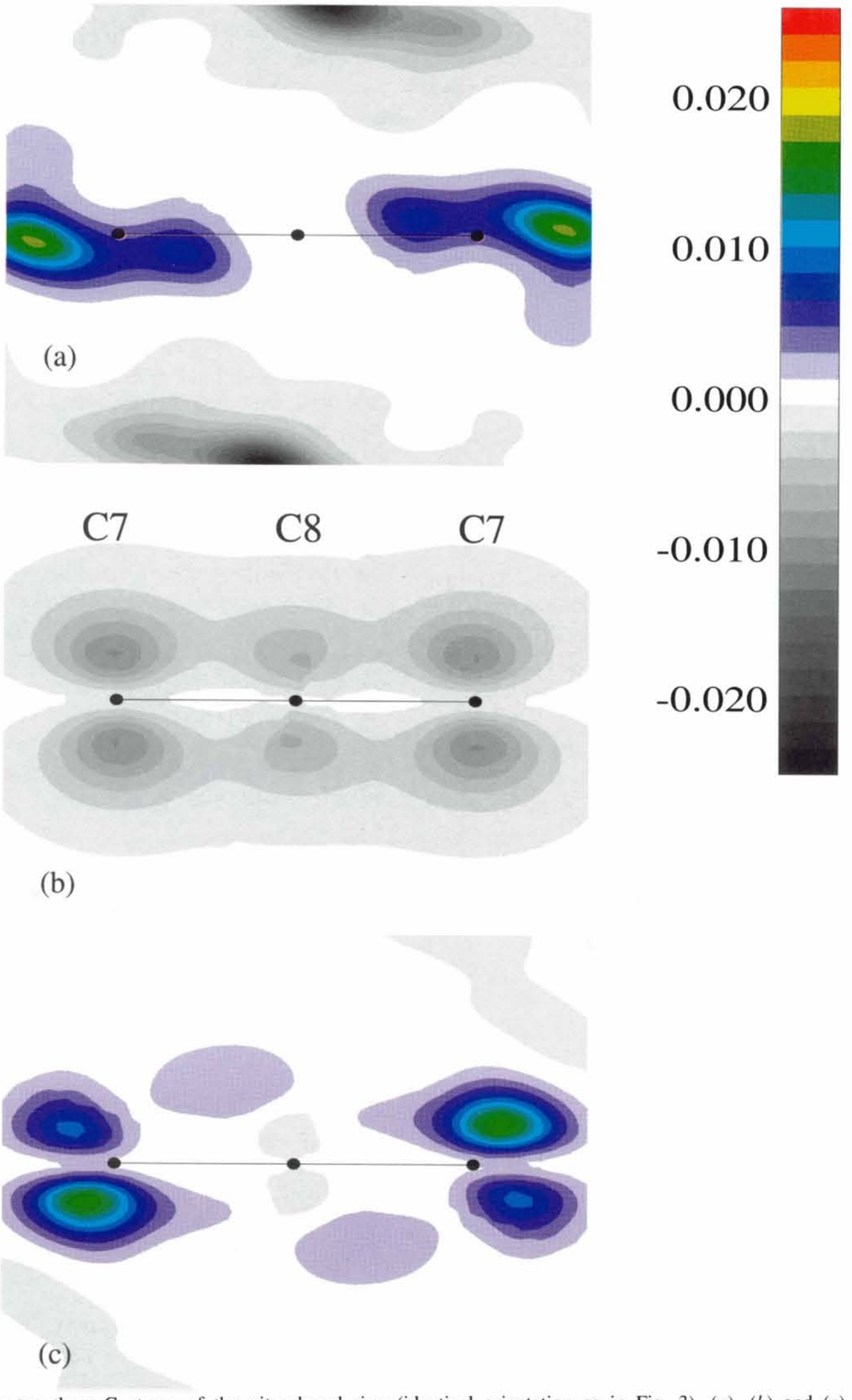

Fig. 4. View onto the top three C atoms of the nitrophenyl ring (identical orientation as in Fig. 3). (*a*), (*b*) and (*c*) refer to the same reconstructions as in Fig. 2. Note that the multipole expansion predicts here a purely negative (albeit small) spin density, whereas the MAXENT reconstruction is mostly positive.

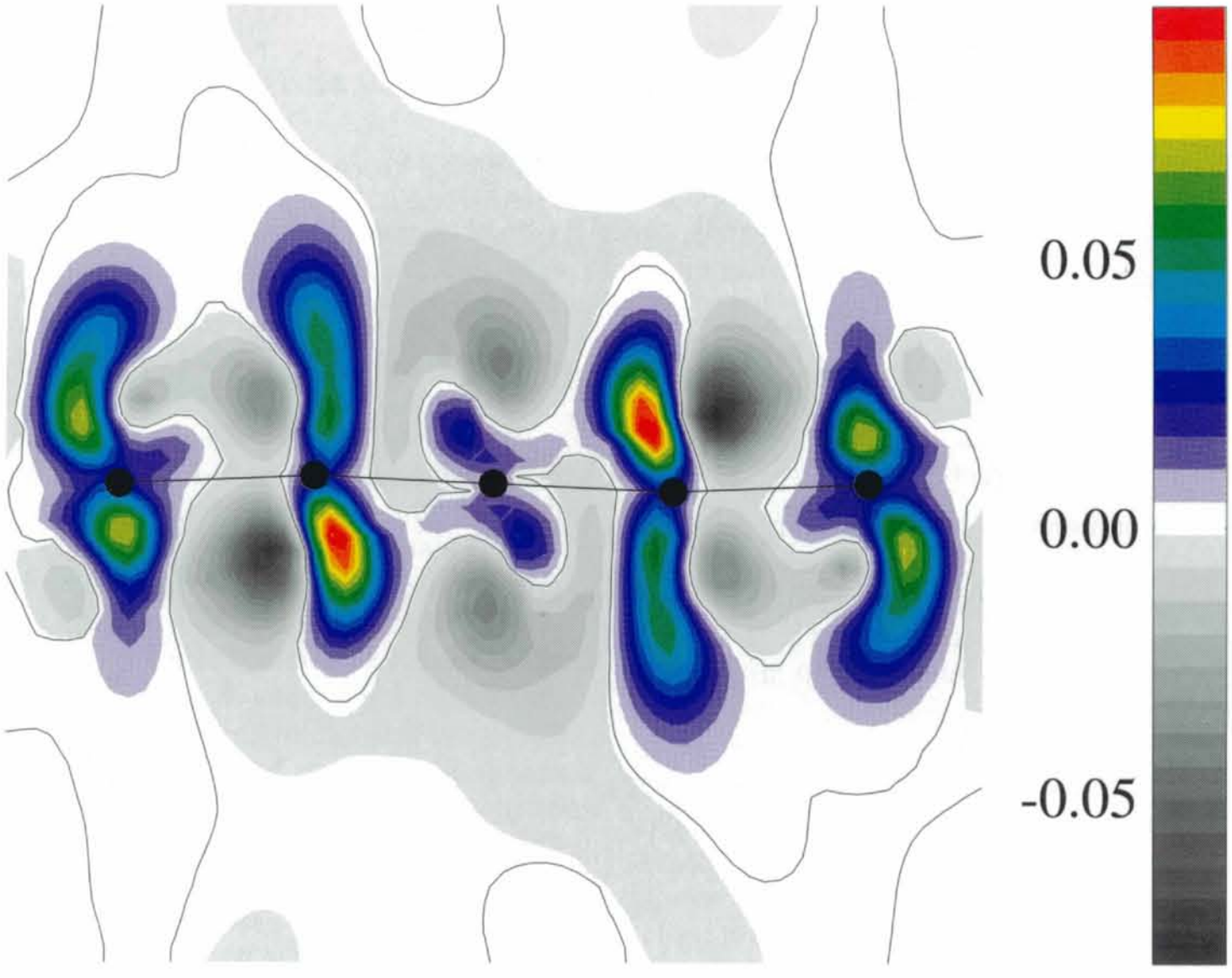

Fig. 5. Spin-density difference between the reconstruction with non-uniform prior (Fig. 3*c*) and the multipole expansion (Fig. 3*b*).

Jauch, W. (1994). *Acta Cryst.* A**50**, 650–652.
Jauch, W. & Palmer, A. (1993). *Acta Cryst.* A**49**, 590–591.
Kinoshita, M. (1993). *Mol. Cryst. Liq. Cryst.* **232**, 1–12.
Kumazawa, S., Kubota, J., Takata, M. & Sakata, M. (1993). *J. Appl. Cryst.* **26**, 453–457.
Kumazawa, S., Takata, M. & Sakata, M. (1995). *Acta Cryst.* A**51**, 47–53.
Le, L. P., Keren, A., Luke, G. M., Lu, W. D., Uemura, Y. J., Tamura, M., Ishikawa, M. & Kinoshita, M. (1993). *Chem. Phys. Lett.* **206**, 405–408.
Mohammad-Djafari, A. & Demoments, G. (1993). Editors. *Maximum Entropy and Bayesian Methods*. Dordrecht: Kluwer Academic Publishers.
Nakazawa, Y., Tamura, M., Shirakawa, N., Shiomi, D., Takhashi, M., Kinoshita, M. & Ishikawa, M. (1992). *Phys. Rev. B*, **46**, 8906–8914.
Navaza, J. (1985). *Acta Cryst.* A**41**, 232–244.
Papoular, R. J. & Delapalme, A. (1994). *Phys. Rev. Lett.* **72**, 1486–1489.
Papoular, R. J. & Gillon, B. (1990). *Europhys. Lett.* **13**, 429–434.
Papoular, R. J., Ressouche, E., Schweizer, J. & Zheludev, A. (1993). *Maximum Entropy and Bayesian Methods*, edited by A. Mohammad-Djafari & G. Demoments, pp. 311–318. Dordrecht: Kluwer Academic Publishers.
Sakata, M. & Sato, M. (1990). *Acta Cryst.* A**46**, 263–270.
Sakata, M., Uno, T., Takata, M. & Howard, C. J. (1993). *J. Appl. Cryst.* **26**, 159–165.
Skilling, J. (1988). *Maximum Entropy and Bayesian Methods in Science and Engineering*, Vol. 1+2, edited by G. J. Erickson & C. R. Smith, pp. 173–187. Dordrecht: Kluwer Academic Publishers.
Skilling, J. (1989). Editor. *Maximum Entropy and Bayesian Methods*. Dordrecht: Kluwer Academic Publishers.
Skilling, J. & Bryan, R. K. (1984). *Mon. Not. R. Astron. Soc.* **211**, 111–124.
Smith, C. R. & Grandy, W. T. Jr (1985). Editors. *Maximum Entropy and Bayesian Methods in Inverse Problems*. Dordrecht: Kluwer Academic Publishers.
Steenstrup, S. & Hansen, S. (1994). *J. Appl. Cryst.* **27**, 574–586.
Takata, M., Sakata, M., Kumazawa, S., Larsen, F. K. & Iversen, B. B. (1994). *Acta Cryst.* A**50**, 330–337.
Wilkins, S. W. (1983). *Acta Cryst.* A**39**, 892–896.
Wilkins, S. W., Varghese, J. N. & Lehmann, M. S. (1983). *Acta Cryst.* A**39**, 47–60.
Zheludev, A., Bonnet, M., Ressouche, E., Schweizer, J., Wan, M. & Wang, H. (1994). *J. Magn. Magn. Mater.* **135**, 147–160.
Zheludev, A., Papoular, R. J., Ressouche, E. & Schweizer, J. (1995). *Acta Cryst.* A**51**, 450–455.
Zheludev, A., Ressouche, E., Schweizer, J. & Turek, P. (1994). *Solid State Commun.* **90**, 233–235.
Zhuang, X., Östevold, E. & Haralick, R. M. (1987). *Image Recovery: Theory and Application*, edited by H. Stark, pp. 157–193. Orlando: Academic Press.